



HAL
open science

Normal modes modelling of post-seismic ionospheric oscillations

Juliette Artru, Philippe Lognonné, Elisabeth Blanc

► **To cite this version:**

Juliette Artru, Philippe Lognonné, Elisabeth Blanc. Normal modes modelling of post-seismic ionospheric oscillations. *Geophysical Research Letters*, American Geophysical Union, 2001, 28, pp.697-700. 10.1029/2000GL000085 . insu-03597765

HAL Id: insu-03597765

<https://hal-insu.archives-ouvertes.fr/insu-03597765>

Submitted on 4 Mar 2022

HAL is a multi-disciplinary open access archive for the deposit and dissemination of scientific research documents, whether they are published or not. The documents may come from teaching and research institutions in France or abroad, or from public or private research centers.

L'archive ouverte pluridisciplinaire **HAL**, est destinée au dépôt et à la diffusion de documents scientifiques de niveau recherche, publiés ou non, émanant des établissements d'enseignement et de recherche français ou étrangers, des laboratoires publics ou privés.

Copyright

Normal modes modelling of post-seismic ionospheric oscillations

Juliette Artru, Philippe Lognonné,

Institut de Physique du Globe de Paris, Paris, France

Elisabeth Blanc

Laboratoire de Détection et de Géophysique, Bruyères le Chatel, France

Abstract. Since 1960, several experiments have shown strong perturbations of the ionosphere after earthquakes. For the biggest quakes, Doppler ionospheric soundings have revealed displacements of several tens of meter of the ionized layers E and F. An accurate modelling of these phenomena was however never described.

We present here synthetic displacements of such oscillations and compare it with experimental data. Realistic models of the atmosphere including viscosity are used, as well as realistic Earth and seismic source model. These ionospheric oscillations are computed by normal modes summation taking explicitly into account the coupling between the solid Earth and the open atmosphere. They are associated to the Rayleigh fundamental surface waves. We obtain a good agreement between synthetics and observations, so it should be possible to use this method to study the ionospheric post-seismic perturbations and possibly the high altitude profile of the density and the viscosity of the atmosphere.

Introduction

Various ground-based or satellite observations have shown the generation of atmospheric and ionospheric disturbances by earthquakes. They have been observed either on electromagnetic measurement [Parrot *et al.*, 1993], or on ionospheric soundings [Yuen *et al.*, 1969; Kelley *et al.*, 1985; Blanc, 1985]. They are expected to be observed by the DEMETER satellite, which objectives are the recording of natural and anthropogenic ionospheric disturbances. Most of the post-seismic signals observed can be explained by a dynamic coupling at the solid Earth atmosphere interface: the vertical displacement of the ground, either near the epicenter or due to Rayleigh waves, induces upward propagating waves in the atmosphere. Although the amplitude is very small on the ground, the oscillations are strongly amplified towards the top of the atmosphere because of the exponential decrease of the density with height. The interaction with ionospheric plasma should then produce the disturbances observed on TEC measurements [Calais & Minster, 1995], and the oscillations of the E and F layers shown by ionospheric sounding.

We present here a method to model the post-seismic atmospheric oscillations induced by earthquakes using normal modes summation. This is commonly used in seismology to compute synthetics long period seismograms, given a 1-D spherical solid Earth model and a source mechanism. In this work, we take into account the whole system, *i. e.* the solid

Earth model and an atmospheric model. Both the excitation (quake, explosion) or the observation can be computed at any place in the complete Earth model.

The first step consists in the computation of eigenmodes of the Earth with a viscous atmosphere. The second step is then a generalization of the normal modes summation techniques, where the displacement is not computed at the altitude of the E and F layers.

Theory

Solid Earth coupling with atmosphere

Adding an atmosphere to the solid Earth induces, by continuity of the radial projection of stresses and of the vertical displacement, a coupling between the solid Earth and the atmosphere. Due to the density contrast, the kinetic energy transferred is generally small, but the amplitude of the atmosphere vertical displacement is the same as in the solid Earth. However, if we assume no dissipation mechanism, a strong amplification occurs: the kinetic energy ρv^2 is conserved whereas the density ρ is exponentially decreasing. For a magnitude of 8, surface waves produce typically at teleseismic distance a few millimeters displacement of the ground, and displacement amplitudes reach up to hundred meters at 100 km height. At higher altitude, these displacements are attenuated by the increasing dynamic viscosity of the rarefied atmosphere and are finally completely lost in heat. Realistic models of the atmosphere must therefore take into account both the atmospheric viscosity and the radiative open boundary.

Attenuation mechanisms

In the neutral atmosphere and at low altitude, the perfect gas law is quite realistic especially for the frequency range where we expect some signal (less than 0.05 Hz). At higher altitude, above 100 km, this description has to be refined: viscous and possibly non-linear and thermal effects appear.

The typical frequency domain of the ionospheric perturbations is from 1 to 50 mHz. In this range, viscous dissipation is expected to be important above 100 km high [Piteway & Hines, 1963]. For a frequency ω , using the Hooke approximation, we can write the viscous stress tensor as:

$$\mathbf{T}'_{ij} = i\omega\mu_{vis} \left(\frac{\partial u_i}{\partial x_j} + \frac{\partial u_j}{\partial x_i} - \frac{2}{3}\delta_{ij}(\nabla \cdot \mathbf{u}) \right). \quad (1)$$

Here, u_i is the displacement and μ the dynamic viscosity. This can be treated as an anelasticity case. As the viscous tensor is frequency dependent, an iterative process will be used to solve the eigenmodes equation. The thermal or non-linear effects will be neglected here. We will discuss the validity of this approximation later.

Copyright 2001 by the American Geophysical Union.

Paper number 2000GL000085.
0094-8276/01/2000GL000085\$05.00

Earth and atmosphere model

The model used here is anisotropic PREM [Dziewonski & Anderson, 1981] for the solid Earth, and *U. S. Standard Atmosphere*, [1976] for the atmosphere, considered as a neutral gas up to 150 km height.

Modes computation

Normal modes solution

Let us now compute the normal modes for such an Earth model. The theory is described in details by Lognonné *et al.*, [1998], and we will here just recall the main steps of the computation.

Due to the lack of free surface at the top of the atmosphere, we use an open radiating surface, following Unno [1989] and Watada [1995], and assume a local dependence of the modes at the top of the atmosphere as r^λ . As shown by Lognonné *et al.*, [1998], each eigenfrequency ω is then associated with two values of λ , respectively associated to modes with upward propagating energy and downward propagating energy. We then select the upward propagating solution, and apply a mapping which allows us to transform a complete basis of test functions u_n chosen as eigenmodes for an elastic Earth model with free surface into a complete basis of test functions v_n for an Earth model with an open radiating condition at frequency ω . The complete set of “free surface modes” computed with the mineos software [Woodhouse, 1988] is taken in this computation, especially with the different types of modes (figure 1) :

- solid modes: these are the “traditional” seismic modes: the energy in the atmosphere is a few per thousand of the total energy.
- atmospheric acoustic and gravity modes: nearly all the energy is in the atmosphere. Group velocities are about 0.01 and 0.2 $km.s^{-1}$ respectively.
- oceanic modes, corresponding to tsunami modes.

Note that at high angular order, the first acoustic branch corresponds to modes trapped at the atmosphere top free surface and are an artefact of the free-boundary condition.

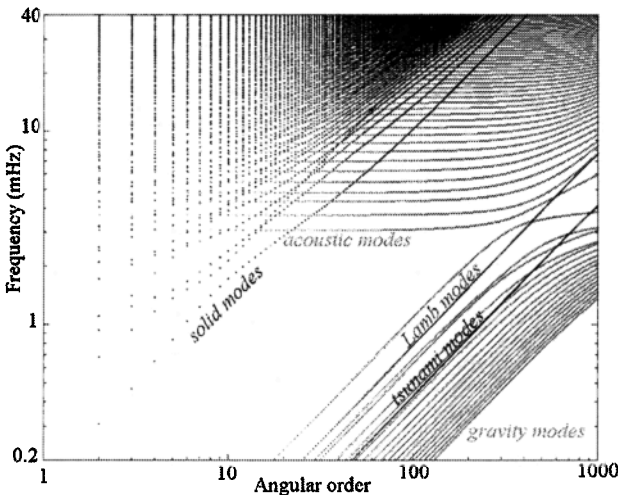


Figure 1. Normal mode basis obtained by minos software, using PREM+USSA model. Gray dots are solid modes, light gray dots are acoustic, Lamb and gravity atmospheric modes, black dots are oceanic modes.

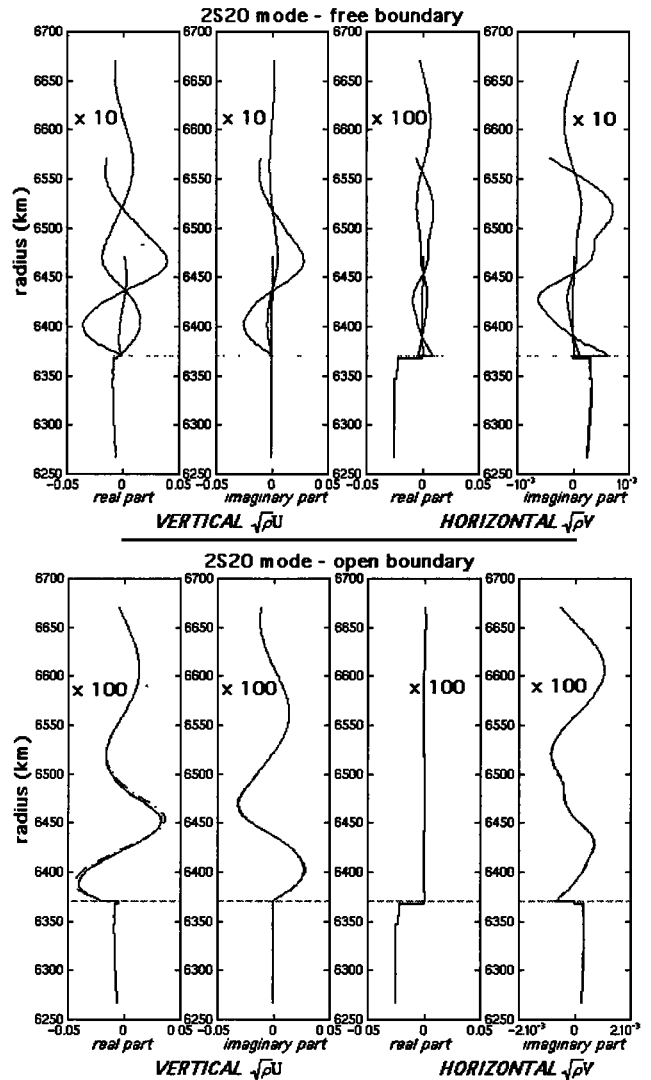


Figure 2. Influence of the boundary condition on the modes. The figure represents the solid modes 2 S 20 computed for 100, 200 and 300 km thick atmosphere models with free (top) and radiative (bottom) boundary conditions. The variation of $\rho^{1/2}U$, where U is the displacement, is shown with respect to the distance to the center of the Earth, and the amplitudes are multiplied by 10 or 100 in the atmosphere (above 6371 km).

The final step consists then in an iterate solution of the eigenmode problem

$$-\omega^2 \mathbf{v} = \mathbf{A}(\omega) \mathbf{v} \tag{2}$$

where $\mathbf{A}(\omega)$ is the elastodynamic operator with the frequency dependent and complex stiffness tensor associated to attenuation in the solid Earth (following Liu *et al.* [1975]), and to the viscosity in the atmosphere following (1). In this eigenmode problem, we practically search the solution as

$$|\mathbf{v}\rangle = \sum c_n \mathbf{v}_n^1, \tag{3}$$

and solve (2) as a variational problem. Note that in this last stage, the first acoustic mode is effectively shifted above the Lamb mode branch.

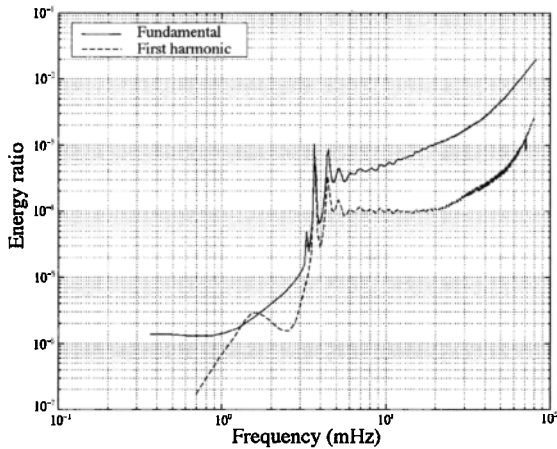


Figure 3. This figure shows the energy ratio in the atmosphere, for the fundamental and first harmonic branches of solid modes. Two peaks at 3.7 and 4.4 mHz are due to a strong coupling with the first acoustic branches.

Realistic modes

The figure 2 shows the differences between the free-boundary and the open-boundary modes. We computed the modes with three different atmospheric thicknesses: 100, 150 and 200 kilometers. The good superposition of the open boundary modes shows that the computation does not introduce an error due to the top of the model.

On the figure 3 the energy ratio in the atmosphere is plotted for the two first solid branches. Two peaks at 3.68 and 4.3 mHz are connected to the frequencies of the first two atmospheric acoustic modes.

Synthetics and data comparison

Data: Doppler ionospheric sounding

We illustrate the method by comparing synthetics with data for the Mexican Earthquake of September, 19, 1985 ($M_w = 7.7$, lat = 18.18 N, lon = 102.37 W), with the CMT source parameters from *Dziewonski et al.*[1987].

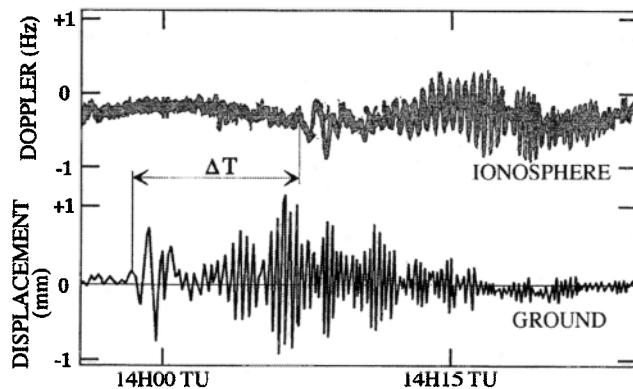


Figure 4. Ionospheric sounding at Francourville after the Mexican earthquake (1985, Sept 19th, $M=7.9$). The Doppler shift observed (about 0.5 Hz) correspond to displacement of the order of 100 m and velocities of about 20 m/s for an ionospheric layer at 150 km height.

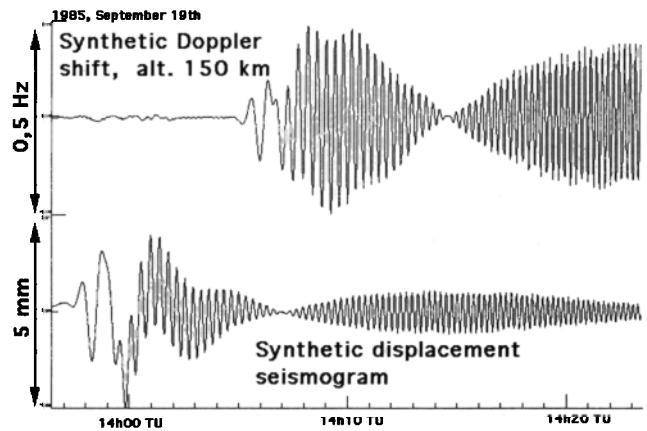


Figure 5. Synthetics computed for the Mexican earthquake. The bottom trace is the synthetic displacement on the ground in Francourville, the top one is the synthetic Doppler shift evaluated from synthetic speed for a frequency of 4.624 MHz.

Perturbations of the ionosphere were observed by Doppler sounding performed at Francourville, near Chartres. Doppler sounding consists in the measurement of Doppler frequency shift between an HF electromagnetic wave ($f_0 = 4.624$ MHz) emitted from the ground and its counterpart reflected on the ionosphere. The reflection altitude depends on the electron density profile (reflection occurs when plasma frequency is equal to wave frequency), and the Doppler shift is related to the vertical velocity v of the reflecting layer as:

$$\delta f = -2f_0 \frac{v \cos(\theta)}{c}, \quad (4)$$

where θ is the zenithal angle of the ray. Figure 4 shows the Doppler measurement. The amplitude of the Doppler shift oscillations reaches 1 Hz peak to peak, which corresponds to a displacement of about 100 m, a speed of 20 m/s, for an altitude of 150 km.

Mexican earthquake: synthetics

Synthetics Doppler diagrams are presented on the figure 5. The arrival time and amplitude at 150 km high are in

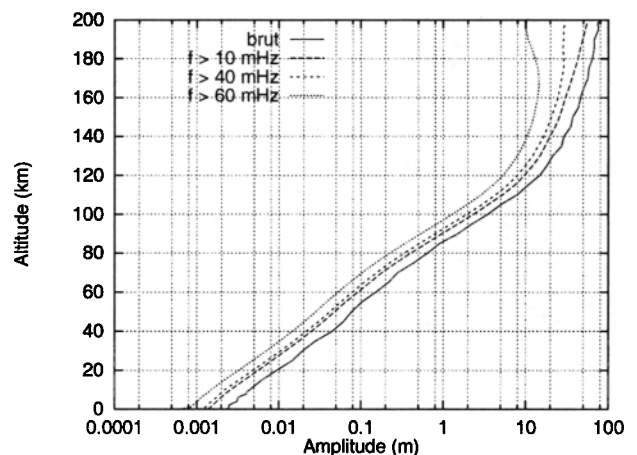


Figure 6. Synthetic displacement maximum amplitude versus height. The figure shows the amplification of the wave in the atmosphere. Attenuation due to viscosity becomes important above 100 km height, which is coherent with previous studies.

good agreement with the Doppler sounding data. Because of the lack of digital data for this earthquake, it is difficult to judge the agreement in the spectral range. The higher frequencies are less attenuated on the synthetics, probably due to the underestimation by our model of the attenuation and surface wave scattering effect. Figure 6 shows the displacement amplitude of the wave versus height, for different frequency ranges. The viscous attenuation appears first for the higher frequencies at about 100 km height. The non-linear terms, neglected during the computation, can be estimated: of the order of $\mathbf{v} \cdot \nabla(\mathbf{v}) \sim \frac{\omega^2 \mathbf{u}^2}{cT}$, they can be compared to $\omega^2 \mathbf{u}$. For $\mathbf{u} \sim 100$ m, $f \sim 50$ mHz, $c \sim 1000$ m/s, we get a ratio of 0.5%, which confirms the linear approximation as still valid.

Conclusion

This computation allows us to model perturbations in the atmosphere induced by coupling with solid Earth. Despite several assumptions made in the atmosphere, we have obtained good preliminary results for post-seismic signals. This method should also permit to study other coupling phenomena like those recorded during volcanic eruptions, atmospheric explosions or tsunami waves. Concerning the thermal or electromagnetic perturbations of the ionosphere observed after earthquakes, they result from non-linear coupling with heat or Maxwell equations, so it is difficult to process them with normal modes theory. However, our computation can be used to produce boundary conditions in ionospheric plasma modelling software.

Acknowledgments. This is IGP contribution 1694. We thank C.-V. Meister and anonymous reviewers for constructive reviews. This work was funded by INSU program PNRN and CNES, in the frame of the DEMETER microsatellite.

References

- Blanc, E., Observations in the upper atmosphere of infrasonic waves from natural or artificial sources: a summary, *Annales Geophysicae*, 3, 6, 673-688, 1985.
- Calais, E., and J.-B. Minster, GPS detection of ionospheric perturbations following the January 17, 1994, Northridge earthquake, *Geophys. Res. Lett.*, 22, 1045-1048, 1995.
- Committee on the Extension to the Standard Atmosphere, *U. S. Standard Atmosphere, 1976*, 227 pp., U. S. Government Printing Office, Washington, D.C., 1976.
- Dziewonski, A., and D. L. Anderson, Preliminary Reference Earth Model, *Phys. Earth Planet. Inter.*, 25, 297-356, 1981.
- Dziewonski, A. M., J. E. Franzen and J. H. Woodhouse, Centroid-moment tensor solutions for July - September 1985., *Phys. Earth Planet. Inter.*, 42, 205-228, 1986.
- Kelley, M. C., Livingston, R., and McCready, M., Large Amplitude Thermospheric Oscillations Induced By Earthquakes, *Geophys. Res. Lett.*, 12, 577-580, 1985.
- Liu, H. P., D. L. Anderson and H. Kanamori, Velocity dispersion due to anelasticity; implications for seismology and mantle composition. *Geophys. J. R. Astron. Soc.*, 47, 41-58, 1975.
- Lognonné, P., E. Clévéde, and H. Kanamori, Computation of seismograms and atmospheric oscillations by normal-mode summation for a spherical earth model with realistic atmosphere, *Geophysical Journal International* 135, 388-406, 1998.
- Parrot, M., J. Achache, J.J. Berthelier, E. Blanc, A. Deschamp, F. Lefeuvre, M. Menvielle, J.L. Plantet, P. Tarits, and J.P. Vilain, High frequency seismo-electromagnetic effects, *Phys. Earth Planet. Inter.*, 77, 65-83, 1993.
- Pitteway, M. L. V., and C. O. Hines, The viscous damping of atmospheric gravity waves, *Can. J. Phys.*, 41, 1935-1948, 1963.
- Unno, W., Y. Osaki, H. Ando, H. Saito, and H. Shibayashi, Non radial oscillations of stars, *Tokyo University Press*, 1989
- Watada, S., Part 1: Near-source acoustic coupling between the atmosphere and the solid Earth during volcanic eruptions, *PhD Thesis, California Institute of Technology, Pasadena*, 1995.
- Woodhouse, J. H., The calculation of the eigenfrequencies and eigenfunctions of the free oscillations of the Earth and the Sun, in *Seismological Algorithms*, edited by D. J. Doornbos, pp. 321-370, 1988.
- Yuen, P.F., P.F. Weaver, R.K. Suzuki, and A.S. Furumoto, Continuous traveling coupling between seismic waves and the ionosphere evident in May 1968 Japan earthquake data, *J. Geophys. Res.*, 74, 2256-2264, 1969.

J. Artru, P. Lognonné, Département des Études Spatiales, Institut de Physique du Globe de Paris, 4 avenue de Neptune, 94107 Saint Maur des Fossés cedex, France. (e-mail: artru@ipgp.jussieu.fr; lognonne@ipgp.jussieu.fr)

E. Blanc, Laboratoire de Détection et de Géophysique, Commissariat à l'Énergie Atomique, BP 12, 91680 Bruyères le Chatel, France. (e-mail: blanc@ldg.bruyeres cea.fr)

(Received April 13, 2000; revised August 10, 2000; accepted October 20, 2000.)